Spectral and spatial transfer and diffusion of excitons in multiple quantum dot structures

S. K. Lyo
Sandia National Laboratories, Albuquerque, New Mexico 87185, USA
(Received 14 August 2008; revised manuscript received 11 December 2008; published 31 March 2009)

A formalism is developed for resonant and nonresonant spectral and spatial energy transfer of excitons in disordered semiconductor multiple-quantum-dot structures. Dipole-dipole and photon-exchange energy-transfer mechanisms are considered. For nonresonant transfer, we study two-site transfer rates in a disordered system as a function of the energy mismatch, the temperature, and the distance. The total time-dependent decay rate of the initial spectral intensity excited at a given energy in the inhomogeneous spectral profile is calculated. For resonant transfer, two-site transfer rates are studied as a function of the distance. The diffusion constant is calculated exactly in a regular quantum dot lattice in order to assess the upper limit of the diffusion constant of a disordered system. We find that the total time-dependent spectral decay rate and the diffusion constant are dominated by the weak long-range photon-exchange interaction mechanism over the standard short-range Förster (dipole-dipole) mechanism in a uniform macroscopic multi-quantum-dot system due to the long mean-free path of the photons.

DOI: 10.1103/PhysRevB.79.125328 PACS number(s): 71.35.Cc, 78.67.Hc, 78.20.Bh

I. INTRODUCTION

Study of the transfer dynamics of excitons between confined systems in semiconductors becomes increasingly important in modern optoelectronic structures such as light emitting diodes (LEDs) and solid-state lighting devices. In these nanostructures, light energy is stored in excitons which can move between two-dimensional (2D) quantum wells (QWs), one-dimensional (1D) quantum wires, or quantum dots (QDs) as well as between confined structures with different dimensions. The physics of exciton transfer between these confined structures is not yet fully studied and is of much practical and academic interest. While exciton transfer between 2D QWs and 1D wires have been studied in the past experimentally[1–3] and theoretically,[1,4–6] exciton transfer between QDs is attracting attention only recently. In this paper, we present a formalism for spectral and spatial energy transfers of excitons in semiconductor multi-quantum-dot systems.

Previous data[1,2] indicate that the exciton transfer rate between distant 2D QWs decays slowly with the distance between the QWs, persisting over a surprisingly long distance, over many tens of nanometers. This intriguing behavior could not be explained[1,2,4] by the standard Förster[7] (i.e., dipole-dipole) transfer mechanism which decays rapidly as $\propto 1/d^4$, where d is the center-to-center distance between the QWs. This behavior was explained recently by the author by showing that while the Förster mechanism dominates the rate at a very short distance (<10 nm), the photon-exchange coupling prevails at a longer distance.[4] This result arises from the fact that the photon-exchange coupling decays slowly with distance and that photons can reach a wide area in the target (i.e., final state) QW, enhancing the efficiency. In the 1D-1D transfer problem, however, the target quantum wire has a small effective cross section due to the narrow dimension in the direction perpendicular to the plane containing both wires, resulting in a poor efficiency for the long-range photon-exchange mechanism in contrast to the 2D-2D case and in agreement with the recent observed data.[3] However, the photon-exchange transfer becomes important in a system consisting of stacks of quantum wires or arrays distributed over a wide range.[6] The importance of photon-mediated energy transfer was recognized early for Frankel excitons in optically active ions in insulators.[8]

Quantum dots are useful for LEDs and solid-state-lighting applications because of their high oscillator strengths arising from the proximity of an electron and a hole narrowly confined inside a QD. Also, localization of excitons in QDs makes it more efficient to emit light than in QWs, where excitons can be mobile. In a system with many QDs, it can take a long time for excitons to diffuse out to the surface and emit light. In this paper, we calculate the resonant and nonresonant interdot energy-transfer rates and show that the photon-exchange mechanism is much more efficient than the Förster mechanism for spectral transfer and spatial diffusion of excitons over a large distance through uniformly distributed QDs owing to (1) the long-range ($\propto 1/r^2$) nature of the photon-exchange transfer rate and (2) the long mean-free paths of the photons.

The organization of the paper is as follows. In Sec. II, we present a basic formalism describing the QD exciton states. The dipole-dipole coupling and photon-exchange interaction mechanisms are described. Their coupling strengths are compared as a function of the distance between the two QDs involved. In Sec. III, resonant and nonresonant transition rates are studied using an elegant diagrammatic technique. Diffusion in a regular QD lattice through incoherent resonant transitions is investigated. Interaction of excitons with acoustic phonons is described. An intuitive perturbation treatment for the phonon-assisted transfer rate is given in a disordered system. Comparisons are made for the diffusion constants and the total spectral transfer rates arising from dipolar and photon-exchange interactions. A brief summary and concluding remarks are given in Sec. IV.

II. BASIC FORMALISM

The exciton wave function in the jth QD is given by[4,9]

$$|j\rangle = v_o \sum_{\mathbf{r}_e,\mathbf{r}_h} F_j(\mathbf{r}_e - \mathbf{r}_j, \mathbf{r}_h - \mathbf{r}_j) a^\dagger_{c,\mathbf{r}_e} a_{v,\mathbf{r}_h} |0\rangle, \tag{1}$$

where v_o is the unit-cell volume, $|0\rangle$ signifies the "vacuum" state with an empty conduction band (c) and a filled valence band (v), and $\mathbf{r}_j$ is the position vector of the center of the QD. The normalized envelope function F_j represents an exciton state of interest and depends on the depths and the shape of the QD. While F_j can be any state inside the jth QD, we will be mainly interested in the ground state for applications. The creation and destruction operators $a^\dagger_{c,\mathbf{r}_e}$ and $a_{c,\mathbf{r}_e}$ ($a^\dagger_{v,\mathbf{r}_h}$ and $a_{v,\mathbf{r}_h}$) create and destroy an electron in the conduction (valence) band at the position $\mathbf{r}_e(\mathbf{r}_h)$ in the Wannier representation. Employing

$$\sum_{\mathbf{r}_\sigma} \to \frac{1}{v_o} \int d^3 r_\sigma, \quad \sigma = e,h, \tag{2}$$

and neglecting the overlap between $|j\rangle$ and $|j'\rangle$, we find $\langle j'|j\rangle = \delta_{j,j'}$.

A. Dipolar interaction

The dipolar coupling is given by[4,9]

$$J_{j,j'} = \frac{C^{\text{dip}}_{jj'}}{r^3_{jj'}} \tilde{D}_{jj'}, \quad \tilde{D}_{jj'} = [\hat{\mathbf{D}}_j \cdot \hat{\mathbf{D}}_{j'} - 3(\hat{\mathbf{r}}_{jj'} \cdot \hat{\mathbf{D}}_j)(\hat{\mathbf{r}}_{jj'} \cdot \hat{\mathbf{D}}_{j'})], \tag{3}$$

where $\mathbf{r}_{jj'} = \mathbf{r}_j - \mathbf{r}_{j'}, r_{jj'} = |\mathbf{r}_{jj'}|, \hat{\mathbf{r}}_{jj'} = \mathbf{r}_{jj'}/r_{jj'}$, $e\mathbf{D}_j$ is the transition dipole moment, $D_j = |\mathbf{D}_j|, \hat{\mathbf{D}}_j = \mathbf{D}_j/D_j$, and

$$C^{\text{dip}}_{jj'} = \frac{e^2 D_j D_{j'} \mathcal{F}_j \mathcal{F}^*_{j'}}{\kappa}. \tag{4}$$

Here, κ is the bulk dielectric constant and $\mathcal{F}_j$ equals $F_j(0)$, where $F_j(\mathbf{k})$ is given by

$$F_j(\mathbf{k}) \equiv \int e^{-i\mathbf{k}\cdot\mathbf{r}} F_j(\mathbf{r},\mathbf{r}) d^3 r. \tag{5}$$

The angular average of $\tilde{D}^2_{jj'}$ with respect to all possible directions of $\mathbf{r}_{jj'}$ is given by

$$\eta^{\text{dip}} = \langle \tilde{D}^2_{jj'} \rangle_{av}: \eta^{\text{dip}}_{\parallel} = \frac{4}{5} \quad \text{for} \quad \mathbf{D}_j \parallel \mathbf{D}_{j'},$$

$$\eta^{\text{dip}}_{\perp} = \frac{9\pi}{32} \quad \text{for} \quad \mathbf{D}_j \perp \mathbf{D}_{j'}. \tag{6}$$

B. Photon-exchange interaction

The exciton-photon coupling part of the Hamiltonian H at jth QD is given for emission by[4]

$$\langle j_0, N_{\nu\mathbf{k}} + 1 | H | j, N_{\nu\mathbf{k}} \rangle = \frac{eE_g}{\hbar c} \left[\frac{2\pi c^2 \hbar (N_{\nu\mathbf{k}} + 1)}{\Omega \epsilon \omega_{\nu\mathbf{k}}} \right]^{1/2} \times e^{i\mathbf{k}\cdot\mathbf{r}_j} \hat{\mathbf{e}}_{\nu\mathbf{k}} \cdot \mathbf{D}^*_j F_j(\mathbf{k}), \tag{7}$$

and for absorption $\langle j, N_{\nu\mathbf{k}} | H | j_0, N_{\nu\mathbf{k}} + 1 \rangle$ by the complex conjugate of this expression. Here, $|j_0\rangle$ denotes the ground state $|0\rangle$ at jth QD, $N_{\nu\mathbf{k}}$ is the equilibrium occupation number of the photon of mode ν and wave vector $\mathbf{k}$, and $\hat{\mathbf{e}}_{\nu\mathbf{k}}$ is the polarization vector. The quantity E_g is the gap energy, Ω is the sample volume, $\hbar\omega_{\nu\mathbf{k}}$ is the photon energy, c is the speed of light, and $\epsilon = n^2$, where n is the refractive index. A relatively small confinement plus binding energy is included in E_g.

Approximating $F_j(\mathbf{k}) \simeq F_j(0) \equiv \mathcal{F}_j$ in view of $|\mathbf{k}\cdot\mathbf{r}| \ll 1$ for nanoscale QDs and using $\Sigma_\nu (\hat{\mathbf{e}}_{\nu\mathbf{k}} \cdot \mathbf{D}_j)^2 = D_j^2 \sin^2\theta$ where θ is the angle between $\mathbf{k}$ and $\mathbf{D}_j$, the exciton radiative lifetime is given by

$$\frac{1}{\tau_{jR}} = \frac{4e^2 k_g^3 D_j^2 \mathcal{F}_j^2}{3\epsilon\hbar}, \tag{8}$$

where $k_g = E_g/(\hbar\tilde{c})$ is the wave number of the gap-energy photon and $\tilde{c} = c/n$. In this paper, numerical applications are made, for example, for $In_xGa_{1-x}As/Al_yGa_{1-y}As$ QDs with small In concentration ($x \ll 1$).[10] Taking $E_g \simeq 1.52$ eV, $D = 5.5$ Å, $n = 3.68$ relevant to GaAs,[11] we estimate $1/\tau_R = 1.48\mathcal{F}_j^2 \times 10^9$ s^{-1}. The above value of E_g ignores the QD-size-dependent confinement and the many-body energy ($\ll E_g$) for simplicity and underestimates the rate τ^{-1}_{jR} somewhat.

An exciton in the jth QD in a state with energy $\varepsilon = \varepsilon_j$ relative to the vacuum-state energy can transfer to another state in the j'th QD through photon-exchange interaction via the following two-step perturbation processes:

$$T_{j,j'} = \sum_{\nu,\mathbf{k}} \frac{\langle j', N_{\nu\mathbf{k}} | H_{\text{e-pht}} | j'_0, N_{\nu\mathbf{k}} + 1 \rangle \langle j_0, N_{\nu\mathbf{k}} + 1 | H_{\text{e-pht}} | j, N_{\nu\mathbf{k}} \rangle}{\varepsilon - \hbar\omega_{\nu\mathbf{k}} - i\Gamma_j}, \tag{9}$$

where $\Gamma_j(\varepsilon)$ is the level damping. In Eq. (9), a photon of wave vector $\mathbf{k}$ and mode ν is emitted in the jth QD in the first step. In the next final step, the same photon is absorbed in the j'th QD. Using Eq. (7), we find

$$T_{j,j'} = \frac{2\pi e^2 E_g^2 D_{j'} D_j^*}{\Omega\epsilon} \sum_{\mathbf{k}} \frac{P_{jj'}(\mathbf{k}) e^{i\mathbf{k}\cdot\mathbf{r}_{jj'}} F_j(\mathbf{k}) F_{j'}(\mathbf{k})^*}{\varepsilon_{\mathbf{k}}(\varepsilon - \varepsilon_{\mathbf{k}} - i\Gamma_j)}, \tag{10}$$

where

$$P_{jj'}(\mathbf{k}) = \sum_\nu (\hat{\mathbf{e}}_{\nu\mathbf{k}} \cdot \hat{\mathbf{D}}_{j'})(\hat{\mathbf{e}}_{\nu\mathbf{k}} \cdot \hat{\mathbf{D}}^*_j), \tag{11}$$

and $\varepsilon_k = \hbar\omega_{\nu\mathbf{k}}$. The main contribution to the $\mathbf{k}$ summation arises from $\varepsilon_{\mathbf{k}} \sim \varepsilon$. Since $|\mathbf{k}|R \ll 1$, where R is radius of the QD, we can replace $F_j(\mathbf{k}) = \mathcal{F}_j$ in Eq. (10). Omitting the subscripts jj', the quantity $P(\mathbf{k}) = P_{jj'}(\mathbf{k})$ is given by[4]

$$P_{\parallel}(\mathbf{k}) = \frac{k_{\perp}^2}{k^2} \quad \text{for} \quad \mathbf{D}_j \parallel \mathbf{D}_{j'}, \tag{12}$$

where $k_{\perp}$ is the component perpendicular to $\mathbf{D}_j$ and

$$P_{\perp}(\mathbf{k}) = -\frac{(\mathbf{k}\cdot\hat{\mathbf{D}}_j)(\mathbf{k}\cdot\hat{\mathbf{D}}_{j'})}{k^2} \quad \text{for} \quad \mathbf{D}_j \perp \mathbf{D}_{j'}. \tag{13}$$

In the following, we consider two simple cases for $T_{j,j'}$.

1. $\mathbf{D}_j \| \mathbf{D}_{j'}$

It is convenient to carry out the $\mathbf{k}$ integration first using $\mathbf{r}_{jj'}$ as the polar axis, while keeping the angle θ between $\mathbf{r}_{jj'}$ and $\mathbf{D}_j$ constant. The angular average over θ over the random direction $\mathbf{r}_{jj'}$ will be carried out later. Defining $\lambda\!\!\!^{-} \equiv 1/k_g, x \equiv k r_{jj'}, a \equiv \varepsilon r_{jj'}/\hbar\tilde{c} \simeq r_{jj'}/\lambda\!\!\!^{-}, \gamma \equiv \Gamma_j r_{jj'}/\hbar\tilde{c}$, and

$$\Theta_0 = 1 + \cos^2\theta, \quad \Theta_2 = 3\cos^2\theta - 1, \tag{14}$$

we find after a lengthy algebra

$$T_{j,j'} = \frac{C_{jj'}^{\text{pht}}}{r_{jj'}} I(r_{jj'}),$$

$$I(r_{jj'}) = \frac{1}{\pi}\int_{-\infty}^{\infty} \frac{F(x)dx}{a - x - i\gamma} \equiv \mathcal{R}(r_{jj'}) + i\mathcal{I}(r_{jj'}), \tag{15}$$

where

$$C_{jj'}^{\text{pht}} = \frac{e^2 E_g^2 D_{j'} D_j^* \mathcal{F}_{j'}^* \mathcal{F}_j}{2\hbar^2 c^2} = \frac{3\hbar}{8k_g\sqrt{\tau_{jR}\tau_{j'R}}}, \tag{16}$$

and

$$F(x) = f_1(x) + f_2(x),$$

$$f_1(x) = \Theta_0 \sin x,$$

$$f_2(x) = -\Theta_2[\sin x + 2\cos x/x - 2\sin x/x^2]. \tag{17}$$

The quantity $|I(r_{jj'})|$ is of the order of unity for all a and $|T_{j,j'}|$ decays as $\lambda\!\!\!^{-}/r_{jj'}$ as a function of the distance between the dots in view of using $k_g = 1/\lambda\!\!\!^{-}$. Thus, the quantity $\lambda\!\!\!^{-}$ serves as the length scale for the photon-exchange interaction. For GaAs, we estimate $\gamma \ll 1$ for $r_{jj'} \ll 1$ cm, $\lambda\!\!\!^{-} = 353$ Å, and $a \sim r_{jj'}/(353\ \text{Å})$. The quantity a becomes large for $r_{jj'} \gg \lambda\!\!\!^{-} \sim 353$ Å.

In the following, we study $I(r_{jj'})$. We find

$$\mathcal{I}(r_{jj'}) = F(a), \quad \mathcal{R}(r_{jj'}) \equiv \mathcal{R}_1 + \mathcal{R}_2,$$

$$\mathcal{R}_i = \frac{1}{\pi}\mathcal{P}\int_0^{\infty} \frac{f_i(x)dx}{a - x}, \quad i = 1,2, \tag{18}$$

where $\mathcal{P}$ signifies the principal part. The quantity $\mathcal{R}_1$ can be rewritten as

$$\mathcal{R}_1 = -\frac{\Theta_0}{\pi}\{\cos a[\pi + \text{si}(a)] - \sin a\,\text{Ci}(a)\}, \tag{19}$$

where

$$\text{Si}(a) = \int_0^a \frac{\sin t}{t}dt, -\text{si}(a) = \int_a^{\infty} \frac{\sin t}{t}dt, -\text{Ci}(a) = \int_a^{\infty} \frac{\cos t}{t}dt. \tag{20}$$

The quantity $\mathcal{R}_2$ is given by

$$\mathcal{R}_2 = \frac{1}{\pi}\int_0^a \left[\frac{f_2(t)}{a-t} - \frac{f_2(a+t)}{t}\right]dt - \frac{1}{\pi}\int_a^{\infty} \frac{f_2(a+t)}{t}dt. \tag{21}$$

The imaginary part equals

$$\mathcal{I} = F(a) = \Theta_0 \sin a + f_2(a). \tag{22}$$

The quantities $|\mathcal{R}_1|$, $|\mathcal{R}_2|$, and $|\mathcal{I}| \sim 1$ are of the order of unity for all a. In the limit $a \gg 1$ for large $r_{jj'} \gg \lambda\!\!\!^{-}$, we find $\mathcal{R}_1 = -\Theta_0 \cos a$, $\mathcal{R}_2 = \Theta_2 \cos a$, and $\mathcal{R} = (\Theta_2 - \Theta_0)\cos a$ in view of $\text{Si(a)} = \pi/2, \text{si(a)} = 0, \text{Ci(a)} = 0$. In this limit, we also find $\mathcal{I}(r_{jj'}) = (\Theta_0 - \Theta_2)\sin a$. This asymptotic regime is the regime of main interest of this paper, where photon-exchange interaction dominates over dipolar interaction.

The total transfer rate is determined by the directional average on θ of

$$\langle |T_{j',j}|^2 \rangle = \frac{|C_{jj'}^{\text{pht}}|^2}{r_{jj'}^2}\eta^{\text{pht}}, \quad \eta^{\text{pht}} = \langle |I(r_{jj'})|^2 \rangle. \tag{23}$$

Using

$$\langle \Theta_0^2 \rangle = \frac{19}{8}, \quad \langle \Theta_2^2 \rangle = \frac{11}{8}, \quad \langle \Theta_0\Theta_2 \rangle = \frac{9}{8}, \tag{24}$$

we find for large $r_{jj'} \gg \lambda\!\!\!^{-}$ and for the case $\mathbf{D}_j \| \mathbf{D}_{j'}$

$$\eta_{\parallel}^{\text{pht}} = \frac{3}{2}. \tag{25}$$

In the opposite limit $r_{jj'} \ll \lambda\!\!\!^{-}$, we find directly from Eq. (15) $\eta_{\parallel}^{\text{pht}} = 19/8$.

2. $\mathbf{D}_j \perp \mathbf{D}_{j'}$

The results in Eqs. (15)–(23) still hold in this case except that Θ_0, Θ_2 should be replaced by

$$\tilde{\Theta}_0 = \cos\theta_1 \cos\theta_2, \quad \tilde{\Theta}_2 = 3\cos\theta_1 \cos\theta_2, \tag{26}$$

where $\theta_1(\theta_2)$ is the polar angle between $\mathbf{D}_j(\mathbf{D}_{j'})$ and $\mathbf{r}_{jj'}$. Taking angular averages again

$$\langle \tilde{\Theta}_0^2 \rangle = 1/4, \quad \langle \tilde{\Theta}_2^2 \rangle = 9/4, \quad \langle \tilde{\Theta}_0\tilde{\Theta}_2 \rangle = 3/4, \tag{27}$$

$\langle \mathcal{R}^2 \rangle = \cos^2 a \langle (\Theta_2 - \Theta_0)^2 \rangle$, and $\langle \mathcal{I}(r_{jj'})^2 \rangle = \sin^2 a \langle (\Theta_2 - \Theta_0)^2 \rangle$, we find

$$\eta_{\perp}^{\text{pht}} = 1 \tag{28}$$

for large $r_{jj'} \gg \lambda\!\!\!^{-}$. At a short distance $r_{jj'} \ll \lambda\!\!\!^{-}$, we find $\eta_{\perp}^{\text{pht}} = 1/4$.

C. Comparison of dipolar and photon-exchange interactions

Combining the results of Secs. II A and II B and assuming that all the relevant physical parameters are site independent, the effective strengths of dipolar and photon-exchange interactions as a function of the distance $r=r_{jj'}$ equal

$$J_{\rm eff}(r)=\sqrt{\langle J_{jj'}^2\rangle}=\frac{3\epsilon}{4\kappa}\frac{\hbar\sqrt{\eta^{\rm dip}}}{\tau_R}\left(\frac{\lambda\!\!\!^{-}}{r}\right)^3,$$

$$T_{\rm eff}(r)=\sqrt{\langle|T_{jj'}|^2\rangle}=\frac{3}{8}\frac{\hbar\sqrt{\eta^{\rm pht}}}{\tau_R}\frac{\lambda\!\!\!^{-}}{r}, \tag{29}$$

with the ratio given by

$$\frac{T_{\rm eff}(r)}{J_{\rm eff}(r)}=\sqrt{\eta}\left(\frac{\kappa}{2\epsilon}\right)(r_{jj'}/\lambda\!\!\!^{-})^2, \tag{30}$$

where $\eta=\eta^{\rm pht}/\eta^{\rm dip}$ is of the order of unity. It is seen that the ratio becomes much larger than unity for $a=r_{jj'}/\lambda\!\!\!^{-}\gg\sqrt{2\epsilon/(\kappa\sqrt{\eta})}\sim 1$, namely, when the distance is much larger than $\lambda\!\!\!^{-}$. The interaction strengths become nearly equal at $r_{jj'}=\lambda\!\!\!^{-}$ and are of the magnitude $\sim 3\hbar/8\tau_R$ $\sim 2.5\times 10^{-4}$ meV for $\tau_R=1\times 10^{-9}$ s. Thomas *et al.*[12] obtained a similar result by solving Maxwell's equation with two identical QDs interacting through the electromagnetic field. This agreement is natural since Coulomb interaction originates from photon exchange.

For the GaAs parameters $\kappa\sim 12.9$, $\epsilon\sim 13.5$, and $\lambda\!\!\!^{-}=353$ Å, the photon-exchange interaction takes over at a long distance $r_{jj'}\gtrsim 510$ Å, as shown in Fig. 1 for $\eta^{\rm pht}=\eta^{\rm dip}=1$ on the left axis. It is clear that the photon-exchange interaction is important for macroscopic multiple QD systems where the exciton diffusion occurs over a large length scale. It will be shown later that the long-range nature of the radiative interaction makes it dominate over the dipolar interaction for spectral and spatial diffusion for a macroscopic sample.

III. ENERGY-TRANSFER RATE

The 2D-2D and 1D-1D transfer rate of excitons between two QWs was developed earlier using a rigorous field-theoretic method in terms of Feynman diagrams.[4,6] An extension to the current zero-dimensional–zero-dimensional (0D-0D) transfer is readily carried out. The main transition rate of an exciton from a state $|j\rangle$ in the jth QD to a state $|j'\rangle$ in the empty j'th QD is given by the bubble diagram[4] shown in Fig. 2(a),

$$W_{j\to j'}\equiv W_{jj'}=\frac{2\pi}{\hbar}\mathcal{H}_{\rm eff}(r)^2\int_{-\infty}^{\infty}e^{-\beta(\varepsilon-\mu_j)}\rho_j(\varepsilon)\rho_{j'}(\varepsilon)d\varepsilon, \tag{31}$$

where $\beta=1/k_BT$, T is the temperature, $\rho_j(\varepsilon)$ is the spectral density at the jth QD, $r=r_{jj'}$, $\mathcal{H}_{\rm eff}(r)^2=\langle|\mathcal{H}_{j,j'}|^2\rangle$, and $\mathcal{H}_{j,j'}$ stands for $J_{j,j'}$ as well as $T_{j,j'}$. The quantity $\mathcal{H}_{\rm eff}(r)$ equals $J_{\rm eff}(r)$ or $T_{\rm eff}(r)$ defined in Eq. (29). In Fig. 2, the solid lines are dressed exciton propagators in the Fermion representation, the curvy line is a phonon propagator, the solid dots

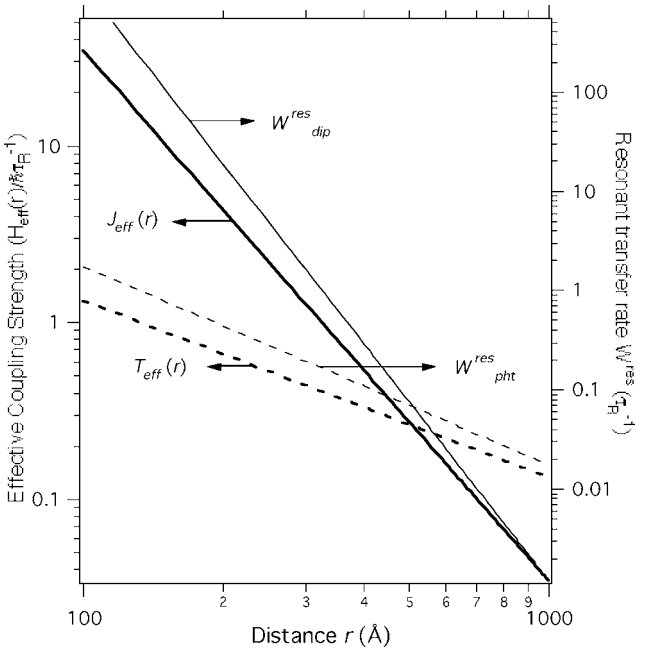

FIG. 1. Comparison of the effective strengths of the dipole-dipole coupling $J_{\rm eff}(r)$ (thick solid curve) and the photon-exchange coupling $T_{\rm eff}(r)$ (thick dashed curve) in Eq. (29) in units of $\hbar\tau_R^{-1}$ for $\eta^{\rm pht}=\eta^{\rm dip}=1$ as a function of the dot-to-dot distance (left axis). The resonant transfer rates in Eq. (36) are displayed on the right axis for $\tau_G=\tau_R$ at zero temperature in units of τ_R^{-1} for dipolar transfer $W^{\rm res}_{\rm dip}$ (thin solid curve) and photon-exchange transfer $W^{\rm res}_{\rm pht}$ (thin dashed curve). The rates are reduced by the factor $\tau_G/\tau_R<1$ at higher temperatures. Other parameters are given in the text.

signify exciton-phonon interaction, and the external vertices with short incoming and outgoing arrows represent dipolar or photon-exchange transition matrix.[4] The quantity $\rho_j(\varepsilon)$ is the imaginary part of the propagator for $|j\rangle$ slightly below the real axis and will be studied below. These diagrams are evaluated with a standard diagrammatic technique.[13,14] The chemical potential μ_j in Eq. (31) enters only the initial site j and is determined by $\exp(-\beta\mu_j)=\Sigma_{j^*}\exp(-\beta\varepsilon_{j^*})$ summed over all intra-QD exciton states $|j^*\rangle$ of the jth QD including

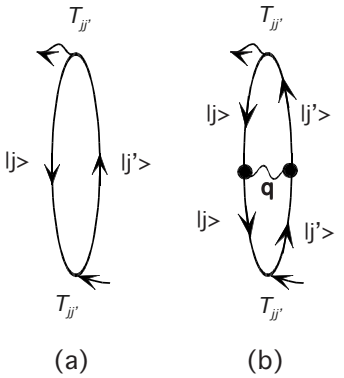

FIG. 2. A bubble (a) and one-rung (b) diagram for the exciton transfer rate. The solid lines indicate exciton propagators in the Fermion representation (Ref. 4) and the curvy line a phonon propagator with a wave vector $\mathbf{q}$. The black dots denote exciton-phonon vertices. The arrows indicate the direction of the energy flow.

the ground level. If there is just one excited level $|j^*\rangle$ with the energy $\varepsilon_j^*=\varepsilon_j+\Delta$ near the ground level ε_j, then we have $\exp[-\beta(\varepsilon_j-\mu_j)]=1/[1+\exp(-\beta\Delta)]$.

In this paper, we assume that the low-lying intradot levels are discrete and do not overlap. In this case, the spectral density around a single level ε_j is given by

$$\rho_j(\varepsilon)=\frac{1}{\pi}\frac{\Gamma_j(\varepsilon)}{(\varepsilon-\varepsilon_j)^2+\Gamma_j(\varepsilon)^2}. \tag{32}$$

When the excited states ε_{j^*} are far away from the ground level ε_j (i.e., $\varepsilon_{j^*}-\varepsilon_j \gg k_BT$), we find $\mu_j=\varepsilon_j$. The expression in Eq. (31) is the microscopic version of the so-called spectral overlap theory,[7,15] with an important explicit energy-dependence for the damping parameter $\Gamma_j(\varepsilon)$ to be studied later. The real part of the self-energy (i.e., the spectral shift) is absorbed into ε_j. A more intuitive perturbation theory to be discussed later gives additional important contribution corresponding to the rate arising from the one-rung diagram shown in Fig. 2(b) as well as the bubble contribution.[4] However, the one-rung diagram does not contribute to the rate in the limit $r_{jj'}$ is much larger than the QD size as will be shown later. This large $r_{jj'}$ regime is relevant to photon-exchange energy transfer.

When the two levels are nearly resonant $|\varepsilon_{jj'}| \lesssim \Gamma_{jj'}$ and $\Gamma_j(\varepsilon), \Gamma_{j'}(\varepsilon)$ are small and slowly varying function of ε in this energy range, we find

$$W_{jj'}=\frac{2\pi}{\hbar}\mathcal{H}_{\mathrm{eff}}(r)^2 e^{-\beta(\varepsilon_j-\mu_j)}\rho_{jj'}(\varepsilon_{jj'}), \tag{33}$$

where $\varepsilon_{jj'}=\varepsilon_j-\varepsilon_{j'}$,

$$\rho_{jj'}(\varepsilon_{jj'})=\frac{1}{\pi}\frac{\Gamma_{jj'}}{\varepsilon_{jj'}^2+\Gamma_{jj'}^2}, \tag{34}$$

$\Gamma_{jj'}=\Gamma_j(\varepsilon_j')+\Gamma_{j'}(\varepsilon_j)$. At very low temperatures $k_BT \ll \Delta$, $\Gamma_j(\varepsilon)$ arises mainly from radiative damping $\Gamma_R=\hbar/2\tau_R$. An additional contribution,

$$\Gamma_j(\varepsilon)=\pi\sum_{j^*,\pm,\mathbf{q}}|\langle j^*,n_{\mathbf{q}}\pm 1|H_{\mathrm{e\text{-}ph}}^j|j,n_{\mathbf{q}}\rangle|^2\delta(\varepsilon-\varepsilon_{j^*}\mp\hbar\omega_{\mathbf{q}}), \tag{35}$$

arises from phonon-assisted damping at higher temperatures. The latter can become large at high temperatures and energy dependent, making the above result less accurate. In Eq. (35), $|j^*\rangle, H_{\mathrm{e\text{-}ph}}^j$, and $n_{\mathbf{q}}$ indicate, respectively, the excited levels (including $|j\rangle$) inside the jth QD, exciton-phonon interaction to be introduced later [with a more explicit form for $\Gamma_j(\varepsilon)$], and the occupation number of the phonon with a wave vector $\mathbf{q}$ and energy $\hbar\omega_{\mathbf{q}}$. The upper (lower) sign corresponds to the transition to $|j^*\rangle$ via one-phonon emission (absorption) from $|j\rangle$. For the case of resonance $\varepsilon_{jj'}=0$, Eq. (33) is rewritten as

$$W_{jj'}^{\mathrm{res}}=e^{-\beta(\varepsilon_j-\mu_j)}\left|\frac{2\mathcal{H}_{\mathrm{eff}}(r)}{\hbar}\right|^2\tau_{j,j'}$$
$$=e^{-\beta(\varepsilon_j-\mu_j)}\left|\frac{2\mathcal{H}_{\mathrm{eff}}(r)\tau_{j,j'}}{\hbar}\right|^2\tau_{j,j'}^{-1}, \tag{36}$$

where $\tau_{j,j'}=\hbar/(2\Gamma_{jj'})\simeq\hbar/[4\Gamma_j(\varepsilon_j)]$ is the phase coherence time for resonance between the two QDs. The expression after the second equality in Eq. (36) illustrates the physical meaning of the result by stating that the resonance transfer rate equals the total transition probability during the coherence time $\tau_{j,j'}$ divided by $\tau_{j,j'}$. Defining the life time τ_G of the exciton ground state by $\tau_G^{-1}=2\Gamma_j(\varepsilon_j)/\hbar=\tau_{j,j'}^{-1}/2$, the resonant transfer rate equals $W_{jj'}^{\mathrm{res}}=2\tau_R^{-1}(\tau_G/\tau_R)|\mathcal{H}_{\mathrm{eff}}(r)\tau_R/\hbar|^2$ for the case $\varepsilon_j=\mu_j$ where only the ground state is relevant. The quantity τ_G^{-1} arises from the radiative damping as well as intradot phonon-assisted transitions. Figure 1 displays $W_{jj'}^{\mathrm{res}}$ in units of τ_R^{-1} on the right axis as a function of the QD-QD separation at zero temperature, where $\tau_G=\tau_R$. This rate is reduced by τ_G/τ_R at high temperatures where intradot "vertical" phonon-assisted transitions dominates τ_G^{-1}.

When the two levels are off resonant i, e, $|\varepsilon_{jj'}| \gg \Gamma_{jj'}$ and $\Gamma_j(\varepsilon)$ and $\Gamma_{j'}(\varepsilon)$ are slowly varying function of ε near ε_j and $\varepsilon_{j'}$, Eq. (31) yields

$$W_{jj'}=\frac{2\pi}{\hbar}\xi|\mathcal{H}_{\mathrm{eff}}(r)|^2[e^{-\beta(\varepsilon_{j'}-\mu_j)}\rho_j(\varepsilon_{j'})+e^{-\beta(\varepsilon_j-\mu_j)}\rho_{j'}(\varepsilon_j)], \tag{37}$$

where the two terms arise from the two distinct poles at $\varepsilon=\varepsilon_j,\varepsilon_{j'}$ and $\xi=1$. It will be shown later that a significant phonon-assisted energy-transfer rate exists only between two QDs with a small energy mismatch (~ a few meV) and therefore the two poles overlap significantly within the energy scale of damping. In this case, the two terms in Eq. (37) amount to double counting of the contributions of each pole. A later full numerical calculation demonstrates that roughly $\xi\simeq 1/2$ as expected. In the rest of this paper, we consider only the simple case $\varepsilon_j=\mu_j$, assuming that all excited levels are outside the thermal reach of $|j\rangle$. We will also consider energy transfer only between the ground-state exciton levels hereafter for simplicity since our treatment can be readily extended to more complex situations. Equation (35) then yields

$$\Gamma_j(\varepsilon)=\pi\sum_{\pm,\mathbf{q}}|\langle j,n_{\mathbf{q}}\pm 1|H_{\mathrm{e\text{-}ph}}^j|j,n_{\mathbf{q}}\rangle|^2\delta(\varepsilon-\varepsilon_j\mp\hbar\omega_{\mathbf{q}}). \tag{38}$$

Using this expression and detailed balance for the first term in Eq. (37), this equation can be rewritten as

$$W_{jj'}=\frac{2}{\hbar}\xi|\mathcal{H}_{\mathrm{eff}}(r)|^2\left[\frac{\Gamma_j(\varepsilon_j+\varepsilon_{jj'})}{\varepsilon_{jj'}^2+\Gamma_j(\varepsilon_{j'})^2}+\frac{\Gamma_{j'}(\varepsilon_j)}{\varepsilon_{jj'}^2+\Gamma_{j'}(\varepsilon_j)^2}\right], \tag{39}$$

The quantity $W_{jj'}$ arises from two-step phonon-assisted transfer processes between the dots as will be shown later.

A. Diffusion of excitons on a QD lattice

Here, we compute the diffusion coefficient of the excitons making random walks between QDs on a regular cubic QD lattice through dipolar and photon-exchange interactions, assuming a *resonant* transfer rate with the properties: $\varepsilon_j = \varepsilon_{j'}, W_{j'j} = W_{jj'} = W(\mathbf{r}_{j'} - \mathbf{r}_j)$. We assume a single ground-state level for each dot. We start from the standard master equation,

$$\frac{dP_j(t)}{dt} = \sum_{j'} W_{jj'}(P_{j'}(t) - P_j(t)) = \sum_{j'} W_{jj'}P_{j'}(t) - W_T P_j(t), \tag{40}$$

where $P_j(t)$ is the occupation probability of the jth QD at time t, $W_T = \Sigma_{j'} W_{jj'}$ is the total scattering-out rate independent of j, $W_{jj} = W(0) \equiv 0$ and $P_j(0) = \delta_{j,0}$, namely, the exciton is initially at $j=0$. Defining N as the number of the QD sites in the lattice and expanding

$$W_{jj'} = \frac{1}{N}\sum_{\mathbf{k}} \exp[\mathbf{k}\cdot(\mathbf{r}_{j'} - \mathbf{r}_j)]\mathcal{W}_{\mathbf{k}}, P_{j'} = \frac{1}{N}\sum_{\mathbf{k}} \exp(-\mathbf{k}\cdot\mathbf{r}_{j'})\mathcal{P}_{\mathbf{k}}, \tag{41}$$

and rewriting Eq. (40) as $d\mathcal{P}_{\mathbf{k}}/dt = \mathcal{W}_{\mathbf{k}}\mathcal{P}_{\mathbf{k}} - \mathcal{W}_0\mathcal{P}_{\mathbf{k}}$, we obtain $\mathcal{P}_{\mathbf{k}}(t) = \exp[(\mathcal{W}_{\mathbf{k}} - \mathcal{W}_0)t]$, where $W_T = \mathcal{W}_{\mathbf{k}=0}$. Therefore, we find[16]

$$P_j(t) = \frac{1}{N}\sum_{\mathbf{k}} \exp(-i\mathbf{k}\cdot\mathbf{r}_j)\exp[(\mathcal{W}_{\mathbf{k}} - \mathcal{W}_0)t], \tag{42}$$

where

$$\mathcal{W}_{\mathbf{k}} = \sum_j \exp(i\mathbf{k}\cdot\mathbf{r}_j)W(\mathbf{r}_j). \tag{43}$$

The long-time behavior for $t \to \infty$ arises from the $\mathbf{k} \simeq 0$ region,

$$\mathcal{W}_{\mathbf{k}} = \mathcal{W}_0 - \mathcal{D}k^2 + \mathcal{O}(k^4), \tag{44}$$

which, inserted in Eq. (42), yields a well-known result,

$$P_j(t) = \left(\frac{b}{2\sqrt{\pi\mathcal{D}t}}\right)^3 \exp\left(-\frac{r_j^2}{4Dt}\right). \tag{45}$$

Here, $\mathcal{D}$ is the diffusion constant and b is the lattice constant.

We now compute $\mathcal{D}$ for the rate of the form

$$W_{0,j} = W(r) = \frac{A_n e^{-r/\ell_n}}{r^n}, \tag{46}$$

where $n=2,6$, and $\ell_6 = \infty$. The quantity $\ell_2 \gg b$ is the energy-dependent photon mean-free path. The coefficients A_n are obtained from Eqs. (29) and (36) for resonant transfer

$$A_2 = 4\tau_{j,j'}\left(\frac{T_{\text{eff}}(r)r}{\hbar}\right)^2,$$

$$A_6 = 4\tau_{j,j'}\left(\frac{J_{\text{eff}}(r)r^3}{\hbar}\right)^2 = \frac{\chi^2}{\sqrt{\eta}}\left(\frac{2\epsilon}{\kappa}\right)A_2. \tag{47}$$

These quantities are independent of the site indices j, j' for a quantum dot lattice. Defining ρ_{QD} as the number of QDs per volume and using Eqs. (43) and (44), we find

$$\mathcal{D}_n = \frac{2\pi}{3}\rho_{\text{QD}}A_n\int_{r_{\min}}^{\infty} \frac{e^{-r/\ell_n}}{r^{n-4}}dr, \tag{48}$$

obtaining

$$\mathcal{D}_2 = \frac{4\pi}{3}\rho_{\text{QD}}A_2\ell_2^3, \quad \mathcal{D}_6 = \frac{2\pi\rho_{\text{QD}}A_6}{3r_{\min}}. \tag{49}$$

Here, the minimum distance is $r_{\min} \sim a$. The ratio equals

$$\frac{\mathcal{D}_2}{\mathcal{D}_6} = \frac{2A_2 r_{\min}\ell_2^3}{A_6} = \frac{\eta}{2}\left(\frac{\kappa}{\epsilon}\right)^2 r_{\min}\ell_2^3 k_g^4. \tag{50}$$

For GaAs QDs, estimate

$$\frac{\mathcal{D}_2}{\mathcal{D}_6} \sim 2.92\,\eta\frac{r_{\min}}{10^2\ \text{Å}}\left(\frac{\ell_2}{10^3\ \text{Å}}\right)^3.$$

For the minimum QD separation of $r_{\min} = 300$ Å, this ratio becomes $\mathcal{D}_2/\mathcal{D}_6 = \eta$ for $\ell_2 = 485$ Å and becomes drastically larger for a larger ℓ_2. A numerical estimate to be presented later shows $\ell_2 \sim 5.1\times 10^3$ Å for resonant transfer at low temperatures, yielding $\mathcal{D}_2/\mathcal{D}_6 \gg 1$. In order to evaluate $\mathcal{D}_2$ in Eq. (49), we assume a purely radiative damping that yields $\tau_{jj'} = \tau_R/2$ for Eq. (47) at low temperatures and employ Eq. (67) for ℓ_2 to be introduced later. We then find $\mathcal{D}_2 = 3\eta^{\text{pht}}\ell_2^2/4\tau_R$ in view of Eqs. (29) and (47) as expected from a scaling argument. The underlying physics states that long-range slow jumps via photon-exchange transfer dominates over the short-range fast dipolar jumps for the random walk of the excitons over the dots in diffusing over a long distance out to the sample surface.

The result in Eq. (48) has a simple qualitative interpretation in terms of a random walk on a lattice. The diffusion constants for a random walk with a unit step length r and a concomitant rate $W_n(r)$ is given by

$$\mathcal{D}_n \sim \sum_{\mathbf{r}} W_n(r)r^2 = 4\pi\rho_{QD}\int_{r_{\min}}^{\ell_n} \frac{A_n}{r^{n-4}}dr, \tag{51}$$

indicating that long- (short-) range transfer dominates the diffusion constant for $n=2(n=6)$.

The results in Eqs. (48) and (51) clearly show that many QDs contribute to the diffusion constant through long-range transfer for the photon-exchange mechanism. Therefore, spatial disorder of the QDs and energy-level disorder are not expected to alter the diffusion constant drastically because excitons can always find resonant sites through the long-range transfer. More specifically, the long-range radial dependence of the photon-exchange transfer rate $\propto r^{-2}$ allows the exciton in question to find a resonant site without fail even in a disordered system at a long distance within a volume shell dr with a probability r^2dr which overcomes the $\propto r^{-2}$ decay of the transfer rate. In contrast, for the short-range dipolar transfer rate $\propto r^{-6}$, the dot-to-dot transfer rate depends sensitively on the energy mismatch and the distance between two nearest neighbors. As a result, slowest links dominate the diffusion process for dipolar transfer and the diffusion constant $\mathcal{D}_6$ in Eq. (49) is an overestimate for a disordered system.

B. Phonon-assisted exciton transfer in a disordered system

Here, we present a perturbation treatment for the energy-transfer rate in a disordered system and quantify $\Gamma_j(\varepsilon)$. In the presence of disorder of the QD sizes, the energy mismatch between the initial and final levels can be significant, requiring phonon-assisted energy transfer. We assume that the magnitude of the disorder energy is smaller than the Debye energy of the acoustic phonons. The role of the LO-phonons is restricted here because of the discrete nature of the QD levels. The electron-phonon interaction due to a deformation potential is given by

$$H_{\text{e-ph}} = \sum_{\sigma,\mathbf{r}_\sigma,s,\mathbf{q}} \exp(i\mathbf{q}\cdot\mathbf{r}_\sigma) V_{\sigma s} a^\dagger_{\sigma\mathbf{r}_\sigma} a_{\sigma\mathbf{r}_\sigma} (b_{\mathbf{q}} + b^\dagger_{-\mathbf{q}}), \quad (52)$$

where $q=|\mathbf{q}|, V_{\sigma s}=\delta_{s,\ell} D_\sigma \Lambda_{\ell q}, \Lambda_{\ell q}=(\hbar q/2\rho_M c_\ell \Omega)^{1/2}$, c_ℓ is the sound velocity of the longitudinal phonons, D_σ is the deformation-potential coefficient in the conduction ($\sigma=c$) and the valence ($\sigma=v$) band, $\mathbf{r}_c=\mathbf{r}_e, \mathbf{r}_v=\mathbf{r}_h$, ρ_M is the mass density, Ω is the sample volume, and $b^\dagger_{\mathbf{q}}(b_{\mathbf{q}})$ creates (destroys) a phonon of mode s (suppressed) with a wave vector $\mathbf{q}$ and energy $\hbar\omega_{s\mathbf{q}}=\hbar c_s q$ in the Debye approximation. Here, we distinguish the phonon frequency $\omega_{s\mathbf{q}}$ from the photon frequency $\omega_{\nu\mathbf{k}}$ introduced earlier. The piezoelectric contribution is obtained in Eq. (52) by replacing $V_{\sigma s}$ by $V^{\text{pz}}_s = eh_{14}B_s(\mathbf{q})\Lambda_{sq}/q \equiv \mathcal{D}^{\text{pz}}_s(\mathbf{q})\Lambda_{sq}$, where e, h_{14} are electronic charge, piezoelectric constant, and $B_\ell=3\sin^2\theta\cos\theta/\sqrt{2}, B_t = \sin\theta(8\cos^4\theta+\sin^4\theta)^{1/2}/2$ and summing over the longitudinal ($s=\ell$) and the transverse ($s=t$) modes for an axially symmetric system around the z axis.[17] Here, θ is the polar angle of $\mathbf{q}$. The piezoelectric contribution to $\Gamma_j(\varepsilon)$ turns out to be small as will be shown later.

Using Eqs. (1) and (52), we find

$$\langle j^*|H^j_{\text{e-ph}}|j\rangle = e^{i\mathbf{q}\cdot\mathbf{r}_j}\sum_{\mathbf{q}} V_{jj^*}(\mathbf{q})(b_{\mathbf{q}} + b^\dagger_{-\mathbf{q}}), \quad (53)$$

where

$$V_{jj^*}(\mathbf{q}) = \int d^3r_e d^3r_h F^*_{j^*}(\mathbf{r}_e,\mathbf{r}_h) F_j(\mathbf{r}_e,\mathbf{r}_h)[V_{cs}e^{i\mathbf{q}\cdot\mathbf{r}_e} - V_{vs}e^{i\mathbf{q}\cdot\mathbf{r}_h}], \quad (54)$$

and the parameters j, j^* denote intradot levels in jth QD. Note that $V_{jj^*}(\mathbf{q})$ becomes very small for $q \gg 1/R$, where R is the QD size, severely restricting the available phonons to small number of low-energy phonons for a large QD.

A two-step transfer-matrix element for exciton transfer between the ground states $|j\rangle$ and $|j'\rangle$ via emission (upper sign) and absorption (lower sign) of a phonon of wave vector $\mathbf{q}$ is given by

$$\langle j'|H_\pm|j\rangle = \left(\frac{e^{i\mathbf{q}\cdot\mathbf{r}_j}V_{jj}(\mathbf{q})}{-\varepsilon_{jj'} - i\Gamma_j(\varepsilon_{j'})} + \frac{e^{i\mathbf{q}\cdot\mathbf{r}_{j'}}V_{j'j'}(\mathbf{q})}{\varepsilon_{jj'} - i\Gamma_{j'}(\varepsilon_j)}\right) \times \mathcal{H}_{j,j'}\sqrt{n_{\mathbf{q}} + \frac{1}{2} \pm \frac{1}{2}}, \quad (55)$$

where $\varepsilon_j = \varepsilon_{j'} \pm \hbar\omega_{\ell q}$ and $n_{\mathbf{q}}$ is the Boson factor. The damping parameters are inserted to avoid divergences at $\varepsilon_{jj'}=0$. In the above expression, the exciton-phonon interaction takes place at jth (j'th) QD for the term proportional to $V_j(V_{j'})$ followed (preceded) by exciton transfer through dipolar or photon-exchange coupling. For the photon-exchange interaction $\mathcal{H}_{j,j'}=T_{j,j'}$, the photon energy equals $\varepsilon_{j'}$ (ε_j) for the first (second) term in Eq. (55). The effect of this small energy difference ($\ll$ gap energy) is negligible for $T_{j,j'}$ in Eq. (9).

The transition rate is then given by

$$W_{j,j'} = \frac{2\pi\xi|\mathcal{H}_{\text{eff}}(r)|^2}{\hbar}\sum_{\mathbf{q},\pm}\left\{\frac{|V_{jj}(\mathbf{q})|^2}{\varepsilon^2_{jj'} + \Gamma_j(\varepsilon_{j'})^2} + \frac{|V_{j'j'}(\mathbf{q})|^2}{\varepsilon^2_{jj'} + \Gamma_{j'}(\varepsilon_j)^2} + \left[\frac{e^{i\mathbf{q}\cdot\mathbf{r}_{jj'}}V_{jj}(\mathbf{q})V_{j'j'}(\mathbf{q})^*}{[-\varepsilon_{jj'} - i\Gamma_j(\varepsilon_{j'})][\varepsilon_{jj'} + i\Gamma_{j'}(\varepsilon_j)]} + \text{c.c.}\right]\right\} \times \left[n_{\mathbf{q}} + \frac{1}{2} \pm \frac{1}{2}\right]\delta(\varepsilon_j - \varepsilon_{j'} \mp \hbar\omega_{\mathbf{q}}), \quad (56)$$

where ξ is inserted as discussed earlier for overlapping poles. The first two terms above are identical to the bubble contributions in Eq. (39) if we identify

$$\Gamma_{j'}(\varepsilon) = \pi\sum_{\pm,\mathbf{q}}|V_{j'j'}(\mathbf{q})|^2\left[n_{\mathbf{q}} + \frac{1}{2} \pm \frac{1}{2}\right]\delta(\varepsilon - \varepsilon_{j'} \mp \hbar\omega_{\mathbf{q}}), \quad (57)$$

and the last cross term represents the contribution from a one-rung diagram. This term represents an interference between the two terms in Eq. (55).

A coherent interference can even quench the energy transfer. This situation occurs at a short distance $qr_{jj'} \ll 1$ for a large energy mismatch $|\varepsilon_{jj'}| \gg \Gamma_j, \Gamma_{j'}$ and for similar QDs with $V_{jj} \simeq V_{j'j'}$: these conditions yield $\langle j'|H_\pm|j\rangle = 0$ in Eq. (55) and thereby a vanishing rate. This effect was pointed out earlier[18] and is absent in the spectral overlap treatment.[7,15] On the other hand, the interference term becomes negligible in the limit $r_{jj'} \gg R$. This can be shown qualitatively by noting that (1) small $q \sim 1/R$ values give a negligible rate due to small electron-phonon coupling strengths and small phonon density of states; and (2) the integrand $e^{i\mathbf{q}\cdot\mathbf{r}_{jj'}}$ for the angular integration oscillates rapidly when $r_{jj'}$ is much larger than the QD size. For example, for a spherical QD, $V_{jj}(\mathbf{q})$ depends only on q, yielding

$$\int_0^\pi \sin\theta e^{i\mathbf{q}\cdot\mathbf{r}_{jj'}}d\theta = \frac{2\sin(qr_{jj'})}{qr_{jj'}},$$

which vanishes for $qr_{jj'} \sim r_{jj'}/R \to \infty$.

We have shown that the nonresonant energy-transfer rate depends on $\Gamma_j(\varepsilon)$. In order to gain a qualitative understanding of this quantity, we study $\Gamma_j(\varepsilon)$ briefly in the following by using a parabolic potential[19] $V(\mathbf{r}_e,\mathbf{r}_h) = m_e\omega^2 r_e^2/2 + m_h\omega^2 r_h^2/2$ for the exciton confinement. Here, $m_e(m_h)$ is the effective mass of the electron (hole). The potential $V(\mathbf{r}_e,\mathbf{r}_h) = M\omega^2 r^2_{\text{cm}}/2 + \mu\omega^2 r^2/2$ is then separable into the relative coordinate $\mathbf{r}=\mathbf{r}_e-\mathbf{r}_h$ and the center-of-mass coordinate $\mathbf{r}_{\text{cm}}=\alpha_e\mathbf{r}_e+\alpha_h\mathbf{r}_h$, where $\alpha_e=m_e/M, \alpha_h=m_h/M$, and $M=m_e+m_h$, yielding[19]

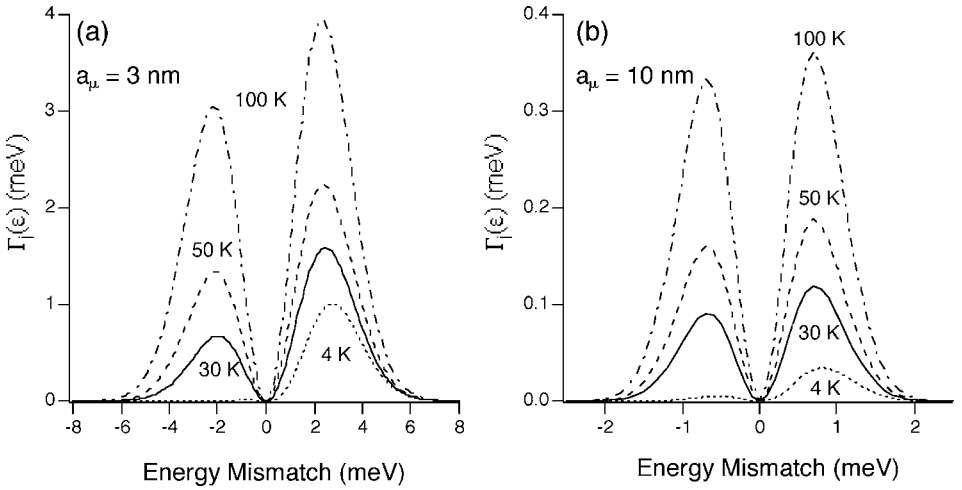

FIG. 3. Damping $\Gamma_j(\varepsilon)=\Gamma_j^{\rm dc}(\varepsilon)+\Gamma_j^{\rm pz}(\varepsilon)$ from one-phonon-assisted transitions calculated from Eqs. (61) and (62) for (a) a small QD with $a_\mu=3$ nm and (b) a large QD with $a_\mu=10$ nm as a function of the energy mismatch $\varepsilon-\varepsilon_j$ for several temperatures. The positive (negative) value of $\varepsilon-\varepsilon_j$ corresponds to Stokes (anti-Stokes) transfer. Other parameters are given in the text.

$$F(\mathbf{r}_e,\mathbf{r}_h)=\frac{1}{(\sqrt{\pi}R)^{3/2}}\exp\left(-\frac{r_{\rm cm}^2}{2R^2}\right)\psi(r), \tag{58}$$

where $R=\sqrt{\hbar/M\omega}$ and ψ is the solution of

$$\left(-\frac{\hbar^2\partial^2}{2\mu\,\partial\,\mathbf{r}^2}+\frac{1}{2}\mu\omega^2r^2-\frac{e^2}{\kappa r}\right)\psi=\varepsilon\psi \tag{59}$$

and μ is the reduced mass. While a desirable variational function is of the form $\psi\propto\exp(-r^2/2a^2-ur)$ where a,u are variational parameters, we employ $\psi=\exp(-r^2/2a^2)/(\sqrt{\pi}a)^{3/2}$ for simplicity, assuming that the QD size is smaller than the Bohr radius $a_B=\kappa\hbar^2/\mu e^2\sim 17.7$ nm for GaAs and thus treating the Coulomb energy as a perturbation. The variational ground state is then given by $a^2\simeq[1-2a_\mu/(3\sqrt{\pi}a_B)]a_\mu^2$ in the limit $a_\mu/a_B\ll 3\sqrt{\pi}/4$, where $a_\mu=(\hbar/\mu\omega)^{1/2}$. We then find from Eq. (54),

$$V_{jj}(\mathbf{q})=\exp(-R^2q^2/4)[V_c\exp(-a^2\alpha_h^2q^2/4) - V_v\exp(-a^2\alpha_e^2q^2/4)]. \tag{60}$$

The deformation-potential contribution is given by

$$\Gamma_j^{\rm df}(\varepsilon)=\frac{q_{\ell\omega}^3}{4\pi\rho_Mc_\ell^2}\exp(-R^2q_{\ell\omega}^2/2) \times(D_ce^{-a^2\alpha_h^2q_{\ell\omega}^2/4}-D_ve^{-a^2\alpha_e^2q_{\ell\omega}^2/4})^2[n_{q_{\ell\omega}}+\Theta(\varepsilon-\varepsilon_j)], \tag{61}$$

where the phonon energy $\hbar c_\ell q_{\ell\omega}$ equals the energy mismatch $|\varepsilon-\varepsilon_j|$ and $\Theta(\varepsilon)$ is the unit step function. Similarly, the piezoelectric contribution equals

$$\Gamma_j^{\rm pz}(\varepsilon)=\sum_s\frac{q_{s\omega}^3\langle\mathcal{D}_s^{\rm pz}(\mathbf{q})^2\rangle_\theta}{4\pi\rho_Mc_s^2}\exp(-R^2q_{s\omega}^2/2) \times(e^{-a^2\alpha_h^2q_{s\omega}^2/4}-e^{-a^2\alpha_e^2q_{s\omega}^2/4})^2[n_{q_{s\omega}}+\Theta(\varepsilon-\varepsilon_j)], \tag{62}$$

where $\hbar c_sq_{s\omega}\equiv|\varepsilon-\varepsilon_j|$ and $\langle\,\rangle_\theta$ denotes the angular average over the polar angle θ: $\langle\mathcal{D}_\ell^{\rm pz}(\mathbf{q})^2\rangle=(12/35)(eh_{14}/q_{s\omega})^2$ and $\langle\mathcal{D}_t^{\rm pz}(\mathbf{q})^2\rangle=(163/560)(eh_{14}/q_{s\omega})^2$.

For a numerical evaluation of $\Gamma_j(\varepsilon)=\Gamma_j^{\rm df}(\varepsilon)+\Gamma_j^{\rm pz}(\varepsilon)$, we use $m_e=0.067m_0, m_h=0.09m_0$ (Ref. 19) and two different effective QD radii: $a_\mu=3$ nm and $a_\mu=10$ nm, where m_0 is the free-electron mass. We also employ $D_c=-6.5$ eV, $D_v=3.1$ eV,[9] $\rho_M=5.3$ g/cm^3, $c_\ell=5.14$ cm/s, $c_t=3.04$ cm/s, and $h_{14}=1.2\times10^7$ V/cm relevant for GaAs.[17] The result is displayed in Fig. 3 for several temperatures for a small QD with $a_\mu=3$ nm in Fig. 3(a) and for a larger QD with $a_\mu=10$ nm in Fig. 3(b). The contribution from piezoelectric scattering is very small ($\sim$ a few percent). There is a severe asymmetry for $\Gamma_j(\varepsilon)$ between the positive (Stokes transfer) and negative (anti-Stokes transfer) values of the energy mismatch $\varepsilon-\varepsilon_j$ at low temperatures. At high temperatures, $\Gamma_j(\varepsilon)$ becomes a more symmetric function of the energy mismatch and becomes linear in T for $k_BT\gg|\varepsilon-\varepsilon_j|$. For small $|\varepsilon-\varepsilon_j|$, $\Gamma_j(\varepsilon)$ rises as $\Gamma_j(\varepsilon)\propto|\varepsilon-\varepsilon_j|^3$ and drops after reaching a peak on both sides, due to the cutoff values of $q\propto1/a$ (which is more severe than $q\propto1/R$) arising from phonon momentum conservation in Eq. (60). Also, a greater number of phonon modes $\mathbf{q}$ with larger energies can interact with smaller QDs, explaining the fact that the magnitude and the energy width as well as the Stokes-anti-Stokes asymmetry is much larger for the smaller QD in Fig. 3(a) than in Fig. 3(b).

The two-site energy-transfer rate is calculated from Eq. (39) for $\xi=1$ using $\Gamma_j(\varepsilon)$ given in Fig. 3 and is displayed in Fig. 4 for several temperature for small QDs with $a_\mu=3$ nm in Fig. 4(a) and for much larger QDs with $a_\mu=10$ nm in Fig. 4(b). The total transfer rate is the product of these spectral rates and the range-dependent part given by the square of the dimensionless coupling strength in Fig. 4(c). In Fig. 4, the quantity τ_R on the vertical axes in Figs. 4(a) and 4(b) cancels τ_R on the vertical axes in Fig. 4(c) and thus may be considered as an arbitrary scaling parameter. It is seen there that spectral transfer takes place more efficiently over a larger energy mismatch between smaller QDs for the same reason as explained above for damping $\Gamma_j(\varepsilon)$. However, the spectral transfer rate for the smaller QDs in Fig. 4(a) is about the same as the rate in Fig. 4(b). The reason behind this surprising result can be seen from Fig. 3. Here, the energy scale of the horizontal axis is not much greater than that of the Γ axis, indicating that the two poles are overlapping and the approximation leading Eq. (31) to the simple convenient result in Eq. (39) is not accurate in the present case.

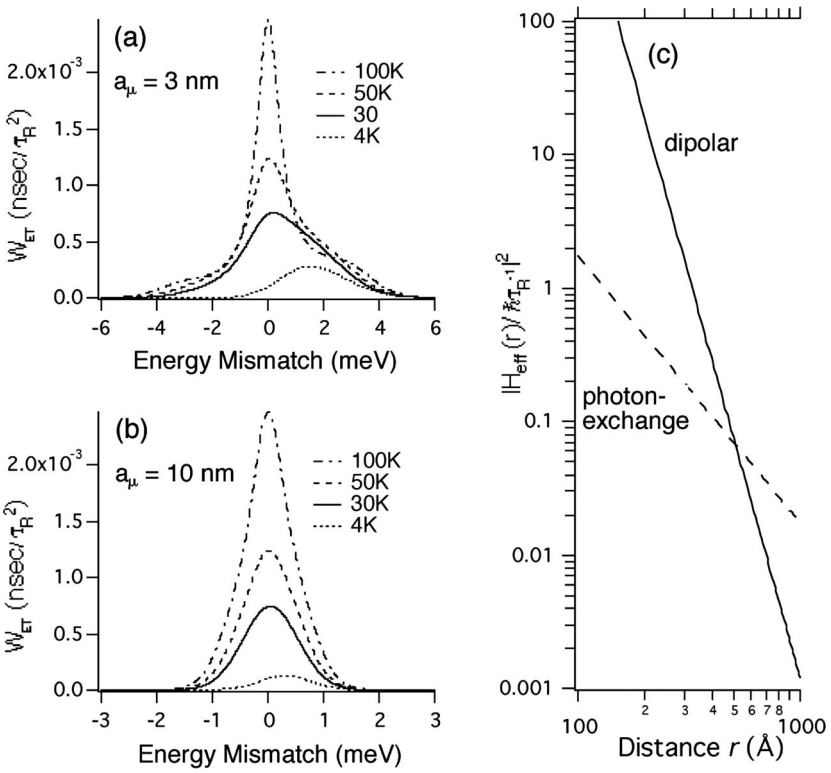

FIG. 4. The spectral part of the two-site energy-transfer rate in units of ns/τ_R^2 calculated from the approximate expression in Eq. (39) for $\xi=1$ as a function of the energy mismatch for (a) small QDs with $a_\mu=3$ nm and (b) much larger QDs with $a_\mu=10$ nm. The positive (negative) value of the energy mismatch corresponds to Stokes (anti-Stokes) transfer. The total rate is the product of these spectral rates and the range-dependent part given by the square of the dimensionless coupling strength in (c). Other parameters are given in the text.

Therefore, we evaluate the two-site transfer rate in Eq. (31) directly. For this purpose, we define $\Gamma_j(\varepsilon)\equiv\Gamma(\varepsilon-\varepsilon_j)$ and rewrite Eq. (31) as

$$W_{jj'}=\left(\frac{\mathcal{H}_{\mathrm{eff}}(r)}{\hbar\tau_R^{-1}}\right)^2\frac{2\hbar\tau_R^{-2}}{\pi}\times\int_{-\infty}^{\infty}e^{-\beta\varepsilon}\frac{\Gamma(\varepsilon)}{\varepsilon^2+\Gamma(\varepsilon)^2}\frac{\Gamma(\varepsilon+\varepsilon_{jj'})}{(\varepsilon+\varepsilon_{jj'})^2+\Gamma(\varepsilon+\varepsilon_{jj'})^2}d\varepsilon. \tag{63}$$

The spectral part of the rate, namely, the quantity that follows the first dimensionless factor $[\mathcal{H}_{\mathrm{eff}}(r)/\hbar\tau_R^{-1}]^2$, is evaluated using $\Gamma(\varepsilon)$ given in Fig. 3 and is plotted in Fig. 5 for several temperature for small QDs with $a_\mu=3$ nm in Fig. 5(a) and for much larger QDs with $a_\mu=10$ nm in Fig. 5(b). The total transfer rate is the product of these spectral rates and the range-dependent part given by the square of the dimensionless coupling strength in Fig. 4(c). Again, the quantity τ_R on the vertical axes in Figs. 5(a) and 5(b) cancels τ_R on the vertical axes in Fig. 4(c) as seen in Eq. (63) and thus may be considered as an arbitrary scaling parameter. The results in Fig. 5 are similar to those displayed in Figs. 4(a) and 4(b) except that they are reduced roughly by a factor of 2 in magnitudes. As mentioned earlier, this factor arises from the double counting of the contributions from the poles at $\varepsilon=\varepsilon_j$ and $\varepsilon=\varepsilon_{j'}$ in Eqs. (37) and (39) when they are close together within the damping width. This correction amounts to setting $\xi\simeq 1/2$. The energy widths are somewhat larger in Fig. 5 than in Fig. 4.

C. Spectral transfer in a disordered multi-QD system

In general, there is some disorder in the size of QDs in a multidot system, giving rise to inhomogeneous broadening of the energy levels. To simplify the problem at this point, we assume that the only relevant disordered quantities are

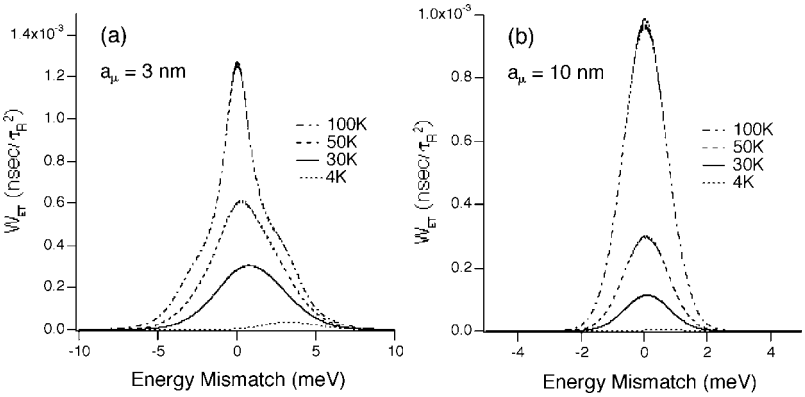

FIG. 5. The spectral part of the two-site energy-transfer rate in units of ns/τ_R^2 calculated from the full expression in Eq. (31) and (63) as a function of the energy mismatch for (a) small QDs with $a_\mu=3$ nm and (b) much larger QDs with $a_\mu=10$ nm. The positive (negative) value of the energy mismatch corresponds to Stokes (anti-Stokes) transfer. The total rate is the product of these spectral rates and the range-dependent part given by the square of the dimensionless coupling strength in Fig. 4(c). Other parameters are given in the text.

the positions and the energy levels of the QDs, neglecting the disorder in the quantities such as $\mathbf{D}_j, \tau_{jR}$, and use the same QD radius for $\Gamma_j(\varepsilon)$ and $\Gamma_{j'}(\varepsilon)$ in Eqs. (61) and (62). The density of states of the levels ε_j of the system is given by $\rho_{\rm QD}g(\varepsilon_j)$ where $g(\varepsilon_j)$ is the normalized inhomogeneous spectral line shape. The transition rate is still given by Eq. (46) except that $A_n(\varepsilon_j-\varepsilon_{j'})$ is a function of the energy mismatch. The coefficient A_2 is given from Eqs. (29), (46), and (63) by

$$A_2(\varepsilon_j-\varepsilon_{j'})=\frac{9\chi^2\eta^{\rm pht}}{32}\frac{\hbar\tau_R^{-2}}{\pi}\int_{-\infty}^{\infty}e^{-\beta\varepsilon}\frac{\Gamma(\varepsilon)}{\varepsilon^2+\Gamma(\varepsilon)^2}\times\frac{\Gamma(\varepsilon+\varepsilon_{jj'})}{(\varepsilon+\varepsilon_{jj'})^2+\Gamma(\varepsilon+\varepsilon_{jj'})^2}d\varepsilon, \tag{64}$$

where $\Gamma_j(\varepsilon)\equiv\Gamma(\varepsilon-\varepsilon_j)$ is the sum of the contributions in Eqs. (61) and (62). A similar expression is obtained for $A_6(\varepsilon_j-\varepsilon_{j'})=A_2(\varepsilon_j-\varepsilon_{j'})(J_{\rm eff}/T_{\rm eff})^2r^4$, yielding

$$A_6(\varepsilon_j-\varepsilon_{j'})=A_2(\varepsilon_j-\varepsilon_{j'})\chi^4(2\epsilon/\kappa)^2/\eta \tag{65}$$

in view of Eq. (30).

An experimentally measurable quantity in the time-resolved optical spectroscopy is the total rate $W_n(\varepsilon)$ with which the initial spectral intensity excited at ε decays in time. The total spectral transfer rate from the jth QD to all other QDs equals

$$W_n(\varepsilon_j)=\sum_{j'}W_{jj'}=\rho_{\rm QD}\int d\varepsilon_{j'}g(\varepsilon_{j'})4\pi\int_{r_{\min}}^{\infty}r^2dr\frac{e^{-r/\ell_n}}{r^n}A_n(\varepsilon_j-\varepsilon_{j'}), \tag{66}$$

where $\ell_6=\infty$ and ℓ_2 is the lesser of the sample size and the photon mean-free path given by[20]

$$\ell_2(\varepsilon)^{-1}=\frac{\pi}{2}\hbar\rho_{\rm QD}k_g^{-2}g(\varepsilon)/\tau_R. \tag{67}$$

For the GaAs parameters, $\rho_{\rm QD}=10^{15}/{\rm cm}^3, \tau_R=0.3\times10^{-9}$ s, and $g(\varepsilon)=0.05/{\rm meV}$, we estimate $\ell_2=0.46$ cm. For resonant transitions on a QD lattice, however, we take $g(\varepsilon)\sim\tau_R/\hbar$, obtaining $\ell_2\sim5.1\times10^3$ Å, assuming a purely radiative linewidth at low temperatures. The quantity ℓ_2 equals $\ell_2(\varepsilon_j)$ $[\ell_2(\varepsilon_{j'})]$ when the phonon is emitted at j'th (jth) QD although $A_2(\varepsilon_j-\varepsilon_{j'})$ does not depend on the photon energy in view of the fact that the photon-exchange interaction $I(r_{jj'})$ in Eq. (32) is nearly insensitive to a small photon-energy difference $|\varepsilon_{jj'}|\ll E_g$. To put this more explicitly, we rewrite Eq. (66) as

$$W_n(\varepsilon_j)=2\pi\rho_{\rm QD}\int d\varepsilon_{j'}g(\varepsilon_{j'})\int_{r_{\min}}^{\infty}r^{2-n}dr\times\left[\exp\left(-\frac{r}{\ell_n(\varepsilon_j)}\right)+\exp\left(-\frac{r}{\ell_n(\varepsilon_{j'})}\right)\right]A_n(\varepsilon_j-\varepsilon_{j'}). \tag{68}$$

For $n=6$, we find

$$W_6(\varepsilon_j)=\frac{4\pi\rho_{\rm QD}}{3r_{\min}^3}\int g(\varepsilon_{j'})A_6(\varepsilon_j-\varepsilon_{j'})d\varepsilon_{j'}. \tag{69}$$

Assuming $r_{\min}\ll\ell_2<$ sample size, we obtain for $n=2$

$$W_2(\varepsilon_j)=2\pi\rho_{\rm QD}\int d\varepsilon_{j'}g(\varepsilon_{j'})[\ell_2(\varepsilon_j)+\ell_2(\varepsilon_{j'})]A_2(\varepsilon_j-\varepsilon_{j'}), \tag{70}$$

or using Eq. (67),

$$W_2(\varepsilon_j)=2\pi\int d\varepsilon_{j'}\left[\rho_{\rm QD}g(\varepsilon_{j'})\ell_2(\varepsilon_j)+\frac{2k_g^2\tau_R}{\pi\hbar}\right]A_2(\varepsilon_j-\varepsilon_{j'}). \tag{71}$$

Remarkably, this quantity is independent of the QD density unlike $W_6(\varepsilon_j)$ in Eq. (69), which is proportional to $\rho_{\rm QD}^2$ in view of $r_{\min}^3\propto\rho_{\rm QD}^{-1}$. This general result follows from the fact that photons can travel over a long distance until it is captured eventually in a macroscopic system.

The numerical results in Figs. 4 and 5 indicate that the transfer rate $\propto A_n(\varepsilon_j-\varepsilon_{j'})$ becomes small for $|\varepsilon_j-\varepsilon_{j'}|$ much larger than a few meV. Typically $g(\varepsilon)$ has a much larger width than this energy width of $A_n(\varepsilon)$. Therefore, we approximate $g(\varepsilon_{j'})\simeq g(\varepsilon_j), \ell_2(\varepsilon_{j'})\simeq\ell_2(\varepsilon_j)$ in Eqs. (69) and (70), obtaining

$$\frac{W_2(\varepsilon_j)}{W_6(\varepsilon_j)}\simeq\frac{3r_{\min}^3\ell_2(\varepsilon_j)\int A_2(\varepsilon_j-\varepsilon_{j'})d\varepsilon_{j'}}{\int A_6(\varepsilon_j-\varepsilon_{j'})d\varepsilon_{j'}}=\frac{3}{4}\eta\left(\frac{\kappa}{\epsilon}\right)^2r_{\min}^3\ell_2(\varepsilon_j)/\chi^4, \tag{72}$$

in view of Eq. (50). This ratio $W_2/W_6\sim5.5\times10^4$ is very large for $\eta=1, \ell_2=0.46$ cm, $r_{\min}=300$ Å and for the parameters relevant to GaAs QD. In this approximation, Eq. (71) can be rewritten as

$$W_2(\varepsilon_j)=8k_g^2\hbar^{-1}\tau_R\int A_2(\varepsilon_j-\varepsilon_{j'})d\varepsilon_{j'}. \tag{73}$$

Inserting Eq. (64) in Eq. (73), we obtain

$$W_2(\varepsilon_j)=\tau_R^{-1}\frac{9\eta^{\rm pht}}{4\pi}G_0(\beta)G_0(0):$$

$$G_n(\beta)\equiv\int_{-\infty}^{\infty}e^{-\beta\varepsilon}\frac{\varepsilon^n\Gamma(\varepsilon)}{\varepsilon^2+\Gamma(\varepsilon)^2}d\varepsilon. \tag{74}$$

Note that this result is independent of ε_j because we have neglected the variation in $g(\varepsilon)$ within the energy range of effective energy transfer near $\varepsilon=\varepsilon_j$. A first-order correction $\delta W_2(\varepsilon_j)$ to $W_2(\varepsilon_j)$ can be made by expanding $g(\varepsilon_{j'})\simeq g(\varepsilon_j)-\varepsilon_{jj'}g(\varepsilon_j)$ in Eq. (71), yielding

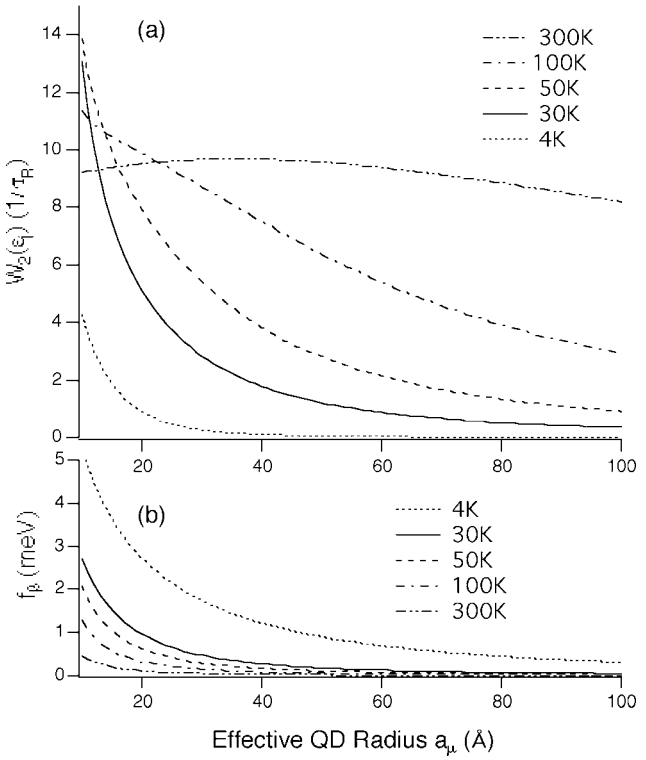

FIG. 6. (a) The total photon-exchange decay rate of the line intensity $W_2(\varepsilon_j)$ in Eq. (74) in units of τ_R^{-1} for a flat spectral density $g(\varepsilon_j)$ as a function of the effective QD radius a_μ for several temperatures. $W_2(\varepsilon_j)$ is independent of the energy ε_j. (b) First-order correction factor f_β in Eq. (75) in units of meV for $g(\varepsilon_j)$ slowly varying in ε_j.

$$\frac{\delta W_2(\varepsilon_j)}{W_2(\varepsilon_j)} = -\frac{g(\varepsilon_j)'}{g(\varepsilon_j)} f_\beta: \quad f_\beta = \frac{1}{2}\left[\frac{G_1(0)}{G_0(0)} - \frac{G_1(\beta)}{G_0(\beta)}\right], \tag{75}$$

where $g(\varepsilon_j)' = dg(\varepsilon_j)/d\varepsilon_j$. The quantities $W_2(\varepsilon_j)$ and f_β are plotted in Fig. 6 as a function of the effective QD radius a_μ for several temperatures. The 100 K (dashed-dotted) curve in Fig. 6(a) crosses over the other lower-temperature curves as a_μ is decreased below 15 Å, because $\Gamma(\varepsilon)$ in the denominator in Eq. (74) becomes large for a small a_μ at high temperatures. As expected, this crossover sets in at a larger a_μ at a higher temperature $T=300$ K (dashed-double-dotted curve).

For a Gaussian line shape,

$$g(\varepsilon) = \frac{1}{\sqrt{2\pi}\sigma}\exp\left(-\frac{\varepsilon^2}{2\sigma^2}\right), \tag{76}$$

where the full width at half maximum equals $W_{fw} \simeq 1.96\sigma$, we find $g'/g = -\varepsilon/\sigma^2$ and

$$\frac{\delta W_2(\varepsilon_j)}{W_2(\varepsilon_j)} = \frac{\varepsilon_j f_\beta}{\sigma^2}.$$

For the energy $|\varepsilon_j| \sim \sigma$ away from the tails of the distribution, the fractional correction in the above expression is small if σ is much larger than a few meV according to the result in Fig. 6(b).

We can calculate the full expression for $W_2(\varepsilon_j)$ in Eq. (71) numerically for a general distribution $g(\varepsilon_j)$. For a Gaussian distribution, we insert Eq. (76) in Eq. (71) and find

$$W_2(\varepsilon_j) = 4k_g^2\hbar^{-1}\tau_R \int_{-\infty}^{\infty} (1 + \exp[-(\varepsilon^2 - 2\varepsilon_j\varepsilon)/2\sigma^2])A_2(\varepsilon)d\varepsilon. \tag{77}$$

Inserting Eq. (64) in Eq. (77), we obtain

$$W_2(\varepsilon_j) = \frac{9\eta^{\text{pht}}}{8\pi}\tau_R^{-1}\int_{-\infty}^{\infty} d\varepsilon' \int_{-\infty}^{\infty} d\varepsilon e^{-\beta\varepsilon}\frac{\Gamma(\varepsilon)}{\varepsilon^2 + \Gamma(\varepsilon)^2} \times \frac{\Gamma(\varepsilon+\varepsilon')}{(\varepsilon+\varepsilon')^2 + \Gamma(\varepsilon+\varepsilon')^2} \times (1 + \exp[-(\varepsilon'^2 - 2\varepsilon_j\varepsilon')/2\sigma^2]). \tag{78}$$

This expression reduces naturally to that in Eq. (74) for a smooth $g(\varepsilon)$ with $\sigma \to \infty$.

Figure 7 displays the spectral decay rate $W_2(\varepsilon_j)$ calculated from Eq. (78) as a function of the energy ε_j for several temperatures for small QDs with an effective radius $a_\mu = 3$ nm for Fig. 7(a) $\sigma = 5$ meV and Fig. 7(b) $\sigma = 10$ meV. Note that the energy dependence of the decay rate is very different for the two cases. In Fig. 7(a) with a narrow distribution width σ, the rate is very asymmetric at low tempera-

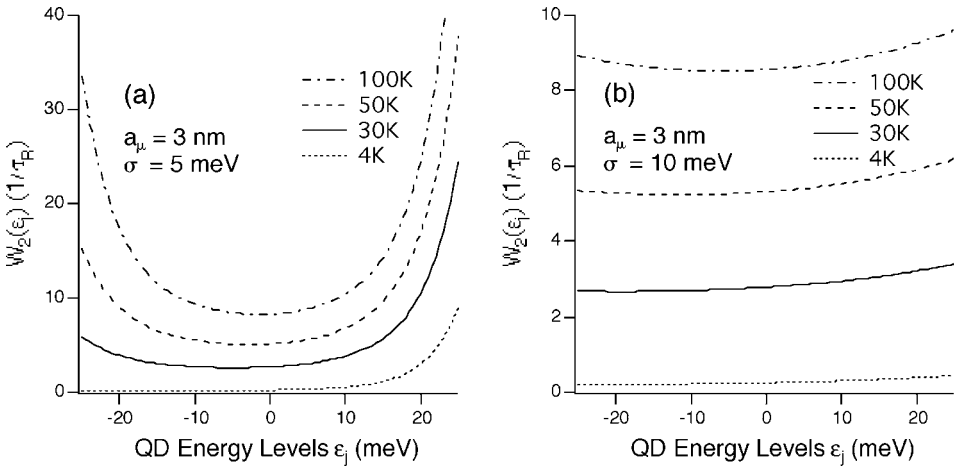

FIG. 7. The total photon-exchange decay rate of the line intensity $W_2(\varepsilon_j)$ in Eq. (78) for small QDs with an effective radius $a_\mu = 3$ nm in units of τ_R^{-1} for a Gaussian spectral density in Eq. (76) as a function of the energy ε_j for several temperatures. The Gaussian function is narrow in (a) $\sigma = 5$ meV and broad in (b) $\sigma = 10$ meV. Other parameters are given in the text.

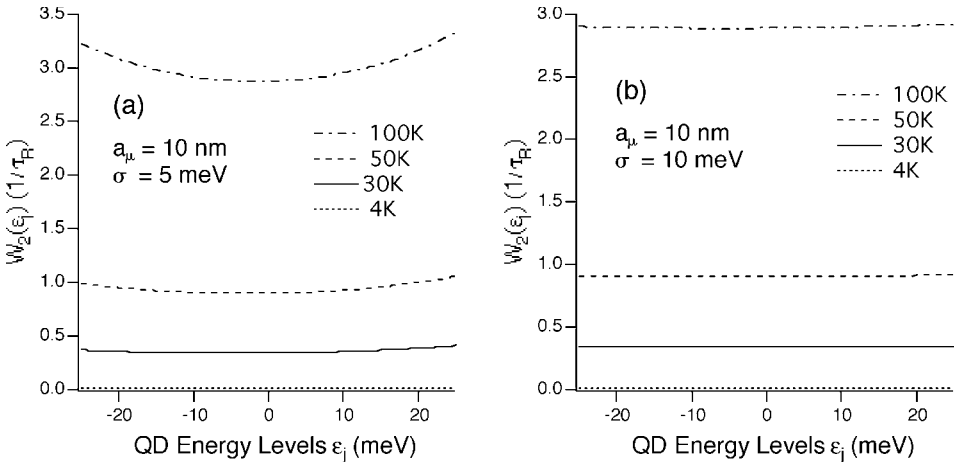

FIG. 8. The total photon-exchange decay rate of the line intensity $W_2(\varepsilon_j)$ in Eq. (78) for large QDs with an effective radius $a_\mu = 10$ nm in units of τ_R^{-1} for a Gaussian spectral density in Eq. (76) as a function of the energy ε_j for several temperatures. The Gaussian function is narrow in (a) $\sigma = 5$ meV and broad in (b) $\sigma = 10$ meV. Other parameters are given in the text.

tures, owing to the fact that it is easier to shift down in energy via phonon emission than to move up in energy through phonon absorption. This asymmetry is still somewhat visible as the rate becomes more symmetric at higher temperatures. In this case, however, the rate at the center of the distribution $\varepsilon_j = 0$ is much smaller than that at the wings because the mean-free path $\ell_2(\varepsilon_j) \propto 1/g(\varepsilon_j)$ in the second term of Eq. (71) is small due to the large density of states $g(\varepsilon_j)$. The energy dependence of $W_2(\varepsilon_j)$ is much weaker for a much broader distribution in Fig. 7(b) as shown in Eqs. (74) and (75).

Figure 8 shows exactly the same plot for $W_2(\varepsilon_j)$ as in Fig. 7 except that the effective QD radius is now increased to $a_\mu = 10$ nm from $a_\mu = 3$ nm. As shown in Fig. 5, the energy range of exciton hopping becomes smaller for larger QDs due to the scaling $q \propto 1/a_\mu$ [cf. Eq. (60)] of the maximum available phonon wave number. Therefore, even a narrow width $2\sigma = 10$ meV of the distribution in Fig. 8(a) is relatively larger than the energy width of effective energy transfer ~4 meV in Fig. 5, yielding roughly the ε_j-independent result for $W_2(\varepsilon_j)$ shown in Eq. (74) approximately. These results apply even better to the wider distribution in Fig. 8(b), where the curves are flat at all temperatures, while the narrower distribution in Fig. 8(a) shows some curvature deviating somewhat from the predictions in Eq. (74).

As mentioned earlier, the total decay rate $W_2(\varepsilon_j)$ via photon-exchange energy transfer is independent of the QD density ρ_{QD} for a macroscopic sample, while $W_6(\varepsilon_j) \propto \rho_{\mathrm{QD}}^2$. When the distribution $g(\varepsilon_j)$ is very broad, $W_2(\varepsilon_j)$ is independent of the energy ε_j as discussed above. However, this is not true for the dipolar rate $W_6(\varepsilon_j)$. In this case, the dependence of the total rate on ε_j is very different as can be shown from Eqs. (67) and (72),

$$W_6(\varepsilon_j) \simeq \frac{2\pi\hbar\rho_{\mathrm{QD}}}{3\tau_R \eta r_{\min}^3}\left(\frac{\epsilon}{\kappa k_g^3}\right)^2 g(\varepsilon_j) W_2(\varepsilon_j) \propto \rho_{\mathrm{QD}}^2 g(\varepsilon_j). \tag{79}$$

Namely, the total transfer rate $W_6(\varepsilon_j)$ is proportional to ρ_{QD}^2 and $g(\varepsilon_j)$ in contrast to $W_2(\varepsilon_j)$.

IV. SUMMARY AND CONCLUDING REMARKS

A field-theoretic formalism was presented for resonant and nonresonant spectral and spatial energy transfer of excitons in semiconductor multi-quantum-dot structures employing dipole-dipole and photon-exchange interactions. While applications were made for energy transfer between the ground exciton states, the formalism is general for transfer from a given state of an initial jth QD to another state in the final j'th QD. This situation becomes important when there are states within a thermal reach from the ground state inside the QDs. We also neglected the distribution of the QD sizes except for generating a distribution of the energy levels. The applications can readily be generalized by employing different expressions for the quantities such as the form factor $F_j(\mathbf{k})$ in Eq. (5) and the damping parameter $\Gamma_j(\varepsilon)$ for different sites, accounting properly for the relevant exciton state and the QD radius. In this case, the thermal weighting factor $\exp[-\beta(\varepsilon - \mu_j)]$ in Eq. (31) represents a thermal average over these initial intradot states as discussed earlier. The photon-exchange coupling was calculated between two QDs and was shown to have a r^{-1} range dependence in contrast to the r^{-3} range dependence of the dipolar interaction. These characteristic radial dependences are general for multilevel QD structures and lead to the dominance of the photon-exchange transfer for the spatial diffusion of excitons over a macroscopic sample and the total spectral transfer rate owing to the long photon mean-free path, a central conclusion of this paper. While dipolar interaction is much stronger than the photon-exchange interaction at short and intermediate distances, the magnitude of the latter dominates the strength of the former roughly beyond $r > \lambda\!\!\!^{-}$ (~353 Å, for example, in GaAs) as shown in Fig. 1.

Resonant transfer rates were calculated as a function of the distance between two QDs and are displayed in Fig. 1 at zero temperature. They can be orders of magnitude greater than the phonon-assisted nonresonant rates shown in Figs. 4 and 5, indicating that the resonant process dominates the exciton diffusion constant except at very high temperatures, where the resonant transfer rate slows down severely due to a very short coherence time τ_G arising from the intradot vertical phonon-assisted transitions to the nearby excited states as discussed earlier. In contrast, nonresonant rates increase

rapidly with the temperature as seen from Figs. 4–8 and can become more important at high temperatures. In order to assess the diffusion constant through resonant transfer, we considered random successive resonant transfer on a regular QD lattice. This model was solved exactly for the diffusion constant. The results are given in Eqs. (48) and (49). We showed, in a regular lattice, that slow but long jumps via photon-exchange coupling yield a much larger diffusion constant than the fast short jumps through dipolar coupling. The advantage of photon-exchange transfer was shown to lie in its long-range radial dependence, which allows excitons to find resonant sites even in a disordered system. Since long-range photon-exchange energy transfer is insensitive to the spectral and spatial disorder, the lattice model is expected to yield a rough estimate of the diffusion constant for a random system for the radiative transfer. For short-range dipolar transfer, however, the lattice model may greatly overestimate the diffusion constant because the diffusion process here is bottlenecked in the percolation chain by slow jumps between resonant pairs of nearest neighbors which happen to have large spatial separations.

For nonresonant transfer, we calculated two-site phonon-assisted energy-transfer rates as a function of the energy mismatch, the spatial separation, the QD radius, and the temperature. The transfer rates and the maximum range of the energy mismatch for efficient transfer were found to be greater for smaller QDs and higher temperatures. Exciton transfer proceeds through incoherent phonon-assisted hopping between QDs. A full expression for two-site resonant and nonresonant transfer rates is given in Eqs. (31) and (63). The interference term introduced in Eq. (56), which corresponds to the one-rung diagram in Fig. 2(b), reduces the net rate at a close distance $r \ll q^{-1}$ between the QDs as discussed earlier, where q is the resonance phonon wave number. The interference term was shown to vanish at a long distance in the opposite regime. The spectral part of the two-site transfer rate calculated from Eq. (63) is displayed in Fig. 5 as a function of the energy mismatch. The results there show that spectral transfer occurs most efficiently for small QDs and over several meV's. The total range-dependent transfer rate at r is given by the product of the rates in Fig. 5 and the dimensionless r-dependent quantity in Fig. 4(c). It is important to point out here that the results presented in Eqs. (63) and (74)–(78) and the concomitant numerical results displayed in Figs. 4–8 are based on the assumption that the QD sizes are not significantly different while there is a distribution in their energy levels, which is a reasonable assumption for typical self-assembled QDs. If there is a significant difference between the sizes of the initial (j) and final (j') QDs, then distinct $\Gamma_j(\varepsilon)$ and $\Gamma_{j'}(\varepsilon)$ should be used for the two sets of Γ's (with different arguments) appearing in the above mentioned equations. In this case, the larger QD will control the exciton-phonon interaction through Eq. (60).

We also proposed that the energy-transfer mechanism can be experimentally studied from the time-dependent decay rate of the initial intensity at a given energy ε_j excited by a sharp laser pulse in a disordered system. This decay rate is the total-energy-transfer rate $W_n(\varepsilon_j)$ from the sites with the energy ε_j to all other sites and was studied as a function of ε_j, the QD radius, the width of the inhomogeneous distribution of the QD levels, and the temperature. A general expression for this rate is given in Eq. (69) for the dipolar rate $W_6(\varepsilon_j)$ and in Eq. (71) for the photon-exchange rate $W_2(\varepsilon_j)$. The latter is independent of the QD density ρ_{QD} in a macroscopic sample and $W_6(\varepsilon_j)$ is quadratic in ρ_{QD}. The total spectral transfer rate is again dominated by the weak long-range photon-exchange interaction mechanism over the standard short-range Förster mechanism for a macroscopic sample [i.e., $W_2(\varepsilon_j) \gg W_6(\varepsilon_j)$]. In a system with a slowly varying spectral density of states, $W_2(\varepsilon_j)$ is independent of ε_j for the photon-exchange transfer, while $W_6(\varepsilon_j)$ is linear in the lineshape function $g(\varepsilon_j)$ for the dipolar rate. The quantity $W_2(\varepsilon_j)$ is given by Eq. (74) for a flat spectral density and is displayed in Fig. 6. This rate is greater for smaller QDs and higher temperatures except for a system with very small QDs, where the rate can decrease for decreasing QD radius at high temperatures as shown by the dashed-double-dotted curve in Fig. 6 at 300 K as discussed earlier. For a Gaussian spectral density of states in Eq. (76), the total spectral decay rate $W_2(\varepsilon_j)$ is given by Eq. (78) and is displayed in Fig. 7 for a system with small QDs and in Fig. 8 for a system with large QDs. The ε_j dependence of $W_2(\varepsilon_j)$ was studied as a function of the temperature and the width of the distribution of the QD levels. A sensitive ε_j dependence of $W_2(\varepsilon_j)$ was found for a system with small QDs with a narrow inhomogeneous distribution of the levels as shown in Fig. 7(a). The rate is greater for smaller QDs and higher temperatures except for very small QDs at high temperatures.

A complete time-dependent solution for the spectral and spatial transport in a system with a random spatial distribution of QDs and a spectral distribution of the exciton levels arising from the fluctuating dot sizes requires a full Monte Carlo simulation, starting with a rate equation based on the basic two-site QD-QD transfer rates obtained in this paper. Photons can escape from the sample either through a spatial diffusion to the surface of the sample or through a spectral diffusion to the wings of the distribution. At the wings of the distribution $g(\varepsilon)$, the photon mean-free path $\ell_2(\varepsilon)$ becomes eventually larger than the sample size according to Eq. (67), allowing the photons with this energy leak out ballistically. A full treatment of this complex problem will be reserved for a future study.

ACKNOWLEDGMENTS

This work was supported in part by LDRD and DOE/BES at Sandia National Laboratories. Sandia is a multiprogram laboratory operated by Sandia Corporation, a Lockheed Martin Co., for the U.S. DOE under Contract No. DE-AC04-94AL85000.

[1] A. Tomita, J. Shah, and R. S. Knox, Phys. Rev. B **53**, 10793 (1996).
[2] D. S. Kim, H. S. Ko, Y. M. Kim, S. J. Rhee, S. C. Hohng, Y. H. Yee, W. S. Kim, J. C. Woo, H. J. Choi, J. Ihm, D. H. Woo, and K. N. Kang, Phys. Rev. B **54**, 14580 (1996).
[3] K. F. Karlsson, H. Weman, K. Leifer, A. Rudra, E. Kapon, and S. K. Lyo, Appl. Phys. Lett. **90**, 101108 (2007).
[4] S. K. Lyo, Phys. Rev. B **62**, 13641 (2000).
[5] S. K. Lyo, Phys. Rev. B **64**, 201317(R) (2001).
[6] S. K. Lyo, Phys. Rev. B **73**, 205322 (2006).
[7] Th. Förster, Ann. Phys. (Leipzig) **2**, 55 (1948).
[8] T. Holstein, S. K. Lyo, and R. Orbach, Phys. Rev. B **16**, 934 (1977).
[9] T. Takagahara, Phys. Rev. B **31**, 6552 (1985).
[10] M. Henini, A. Patanè, A. Polimeni, L. Eaves, P. Main, A. Levin, and G. Hill, Jpn. J. Appl. Phys., Part 1 **40**, 2077 (2001).
[11] *Semiconductors: Group IV Elements and III-V Compounds*, edited by O. Madelung (Springer-Verlag, Berlin, Heidelberg, 1991), p. 101.
[12] P. Thomas, M. Möller, R. Eichmann, T. Meier, T. Stroucken, and A. Knorr, Phys. Status Solidi B **230**, 25 (2002).
[13] T. Holstein, Ann. Phys. (N.Y.) **29**, 410 (1964).
[14] A. L. Fetter and J. D. Walecka, *Quantum Theory of Many-Particle Systems* (McGraw-Hill, New York, 1971).
[15] D. L. Dexter, J. Chem. Phys. **21**, 836 (1953).
[16] D. L. Huber, in *Laser Spectroscopy of Solids*, 2nd ed., edited by W. M. Yen and P. M. Selzer (Springer-Verlag, Berlin-Heidelberg, Germany, 1986) Vol. 49, p. 86.
[17] S. K. Lyo, Phys. Rev. B **40**, 6458 (1989).
[18] T. Holstein, S. K. Lyo, and R. L. Orbach, Phys. Rev. Lett. **36**, 891 (1976).
[19] A more accurate numerical study of the parabolic model is given in W. Que, Phys. Rev. B **45**, 11036 (1992).
[20] A. C. G. Mitchell and M. W. Zemansky, *Resonance and Excited Atoms* (Cambridge University Press, Cambridge, England, 1961), p. 99.